

Supporting Information

Energy-efficient Electrolytic Hydrogen Production Assisted by Coupling Urea Oxidation with pH- gradient Concentration Cell

Genxiang Wang,^{a,b} Junxiang Chen,^a Yan Li,^a Jingchun Jia,^a Pingwei Cai,^{a,b} Zhenhai Wen*,^{a, b}

^aCAS Key Laboratory of Design and Assembly of Functional Nanostructures, and Fujian Provincial Key Laboratory of Nanomaterials, Fujian Institute of Research on the Structure of Matter, Chinese Academy of Sciences, Fuzhou, Fujian 350002, China

^bUniversity of Chinese Academy of Sciences, Beijing 100049, P. R. China

CONTENTS

1. Experimental Section	3
1.1. Materials	3
1.2. Catalyst Synthesis	3
1.3. Materials Characterization	4
1.4. Electrode Fabrication and Electrochemical Measures	5
2. The Effects of pH Difference (ΔpH)	6
3. Theoretical Calculation Details	10
4. Faradic Efficiency for Hydrogen Production	12
5. Figures S1-S23	13
6. Tables S1-S2	37
7. Reference	38

1. Experimental section

1.1 Materials. $\text{CuCl}_2 \cdot 2\text{H}_2\text{O}$ (AR), KOH (AR), urea ($\text{CO}(\text{NH}_2)_2$), $\text{Co}(\text{NO}_3)_2 \cdot 6\text{H}_2\text{O}$ (AR), $\text{Ni}(\text{NO}_3)_2 \cdot 6\text{H}_2\text{O}$ (AR), ammonium hydroxide ($\text{NH}_3 \cdot \text{H}_2\text{O}$, mass fraction of 25%-28%), hydrazine hydrate were purchased from Sinopharm. Graphene aqueous solution (2mg/mL) was prepared from natural graphite powders by a modified Hummer's method,¹ and was diluted into 1mg/mL before using. Nafion (5 %) was purchased from Aladdin. Carbon cloth and Pt/C (20%) were bought from sigma-aldrich. The bipolar membrane was bought from the Yanrun Film Technology Development Co. , Ltd in Beijing. All reagents were used without further purified.

1.2 Catalyst Synthesis.

CuCl/rGO and the Control materials: 25ml GO (1 mg/mL) was dispersed into 50ml H_2O by sonicating half an hour, and 0.2537g $\text{CuCl}_2 \cdot 2\text{H}_2\text{O}$ was dissolved in 25ml H_2O , then cupric chloride solution was added into the GO solution under vigorous stirring and the blue and brown solution was continually stirred for 15min at room temperature, then 0.34mL $\text{NH}_3 \cdot \text{H}_2\text{O}$ (25%-28%) was dripped into the above solution, followed by dropping 0.02 mL $\text{N}_2\text{H}_4 \cdot \text{H}_2\text{O}$. After being vigorously stirred for 10min, the beaker containing solution was put in an oil bath and keep at 95 °C for 1 h. Then the suspended solution was lyophilized to obtain black powers. A porcelain boat with the lyophilized materials was placed in the center of a tubular furnace with raised temperature to 300 °C for 12 h at the heating rate of 3 °C /min under Ar atmosphere and CuCl/rGO was obtained. In this work, rGO was synthesized by the same procedure without adding cupric chloride solution and GO solution, and CuCl

nanoparticles was prepared by the above procedure without addition of GO solution and dispose of oil bath. While CuO/rGO was synthesized by the same procedure with raise temperature to 500 °C at the heating rate of 5 °C /min under Ar atmosphere.

Preparation of CoS₂ and NiSe₂. Firstly, the Co or Ni LDH nanosheet arrays were supported on the carbon cloth (CC) by electrodeposition method. CC was cooked in 0.5 M H₂SO₄ and 30% H₂O₂ at 80 °C for 1h in the oil bath, respectively, and then washed with deionized water and dried for electrodeposition. The electrodeposition solution consists of 0.1 M metal ions. A three-electrode system was used for electrodeposition with a single cycle of deposition consisting of a constant-potential electrodeposition potential at -1.2 V vs. Ag/AgCl for 30 s and a subsequent resting step for 20 s, and the cycle was repeated for 4 times. The obtained Ni LDH/CC and Co LDH/CC were rinsed with deionized water and dried at 60 °C for use. The corresponding Ni LDH/CC or Co LDH/CC in a porcelain boat were put in the hot centre of the tube furnace, and the Se powder (0.2 g for selenization) or S powder (0.5 g for sulfuration) was placed in a suitable location of the upstream, then the tube furnace was heated to 500 °C (for selenization) and 400 °C (for sulfuration) at a heat speed of 2 °C/min and hold 2 hours in Ar atmosphere. After cooling to room temperature, CoS₂/CC and NiSe₂ were obtained.

1.3. Materials Characterization.

The X-ray diffraction (XRD) patterns of materials were obtained at room temperature on a Rigaku Dmax2500 powder X-ray diffractometer using Cu -K α radiation ($\lambda = 1.540598 \text{ \AA}$) in the angular range of $2\theta = 10\text{--}80^\circ$ with a scan step width

of 0.05°. The morphologies and structures of these catalysts were analyzed on the scanning microscopy (SEM, SU-8010) and transmission electron microscopy (TEM, Tecnai F20), and Energy dispersive X-ray spectroscopy (EDS) analysis was also obtained from TEM. The components on the surface of catalysts were determined by X-ray photoelectron spectroscopy (XPS, ESCALAB 250). The Raman spectrums were recorded on a Renishaw in Via Raman Microscope (532). Electrochemical measurements were performed on a CHI 760E electrochemical analyzer (Shanghai, China). The pH value were evaluated on the

1.4. Electrode Fabrication and Electrochemical Measures.

The work electrodes for electrochemical measurements in three-electrode system were fabricated as followings: (i) the glassy carbon electrodes with diameter of 3.0 millimeter were polished using aluminum oxide (Al_2O_3 , 0.05 μm) powder followed by rinsing thoroughly with deionized water and dried at room temperature; (ii) the catalyst ink was obtained by dispersing 5.0 mg catalysts into a mixture of 0.05 mL Nafion, 0.075 mL isopropanol and 0.375 mL deionized water under ultrasonic agitation at least 0.5 h; (iii) then 3 μL of the ink was drop onto the GCE and naturally dried under room temperature. The electrocatalytic properties of the catalysts for urea oxidation were carried out on a three-electrode system on the CHI 760E electrochemical workstation. The three-electrode electrochemical cell was composed of the prepared work electrode, a graphite plate as the counter electrode, and the Ag/AgCl electrode (saturated KCl aqueous solution) as the reference electrode. The electrochemical sweep tests were performed at a potential range of 0 V to 0.8 V (*vs.*

Ag/AgCl). The electrolytes for tests were 1 M KOH in the absence and presence of 0.5 M urea. In order to guarantee a reducible onset of the urea oxidation reaction, twenty cycles in all cyclic voltammetry (CV) measurements were operated on the electrode from 0 to 0.8 V vs. Ag/AgCl at scan rate of 100 mV s⁻¹ before testing at scan rate of 50 mV s⁻¹. The Nyquist plots of Electrochemical Impedance Spectroscopy were recorded in the frequency range of 100 kHz and 0.01 Hz in 1.0 M KOH with 0.5 urea solution at open circuit potential of 0.55 V vs. Ag/AgCl. For two-electrode electrolysis, CuCl/rGO and commercial Pt/C (20%) were drop-casted on carbon cloth (1.0 cm²) with catalysts loading of about 1mg/cm⁻² act as the anode and cathode, respectively. The linear sweep voltammetry (LSV) was scanned at a sweep rate of 5 mV s⁻¹. All measurements were performed at room temperature. All the potentials were quoted with respect to reversible hydrogen electrode (RHE) through RHE calibration according to the formula: $E \text{ (vs. RHE)} = E \text{ (vs. saturated Ag/AgCl)} + 0.197 + 0.0591 * \text{pH}$.

2. The Effects of pH gradient² (ΔpH) between anode and cathode

As known to us all, when the electrolytes in the two chambers are the same, acid, alkaline or neutral solution, the theoretical applied voltage for water splitting is always 1.23 V. However, bipolar membrane allows the sustainable use of distinct electrolyte compositions with different pH in two separate chambers.³ The bipolar membrane is a double-layer membrane that consists of an anion exchanger layer on the cathode side blocking transport of cation and a cation exchanger layer on the anode side of the cell blocking transport of anion, and the K⁺ in anode chamber and

SO₄²⁻ anions in cathode chamber are transported to cation and anion exchanger layer of bipolar membrane, respectively (Figure S13a). And the applied voltage can be tuned by differing pH between the anode chamber and cathode chamber. When HER in 0.5 M H₂SO₄ (pH = 0) as the cathode and OER in 1.0 M KOH (pH = 14) as the anode are assembled in the two chambers forming a pH-gradient concentration cell for water electrolysis, the reactions and its corresponding Nernst equations can be expressed as following:

For water electrolysis in the base-acid electrolyzer:

HER at the cathode:



$$E_{HER} = E_{\text{H}^+/\text{H}_2}^\theta - 2.303 \frac{RT}{2F} \log \left[\frac{\alpha_{\text{H}_2}}{(\alpha_{\text{H}^+})^2} \right] = 0 \text{ V} - 0.059 * \text{pH}_{\text{cathode}} = 0$$

$$\left(E_{\text{H}^+/\text{H}_2}^\theta = 0 \text{ V vs. RHE} \right) \quad (\text{Eq.1})$$

OER at the anode:



$$E_{OER} = E_{\text{O}_2/\text{OH}^-}^\theta - 2.303 \frac{RT}{4F} \log \left[\frac{(\alpha_{\text{OH}^-})^4}{(\alpha_{\text{H}_2\text{O}})^2 (\alpha_{\text{O}_2})} \right] = 1.23 \text{ V} - 0.059 * \text{pH}_{\text{anode}} = 0.404$$

$$\left(E_{\text{O}_2/\text{OH}^-}^\theta = 1.23 \text{ V vs. RHE} \right) \quad (\text{Eq.2})$$

The overall reaction for water splitting:



$$V_{\text{theoretical required}} = E_{\text{O}_2/\text{OH}^-}^\theta - E_{\text{H}^+/\text{H}_2}^\theta - 2.303 \frac{RT}{4F} \log \left[\frac{(\alpha_{\text{H}_2\text{O}})^2 (\alpha_{\text{O}_2}) (\alpha_{\text{H}_2})^2}{(\alpha_{\text{H}^+})^4 (\alpha_{\text{OH}^-})^4} \right]$$

$$= 1.23 - 0.059 * (\text{pH}_{\text{anode}} - \text{pH}_{\text{cathode}}) = \mathbf{0.404} \quad (\text{Eq.3})$$

In these equations, F is the faraday constant, $96\,485\text{ C mol}^{-1}$, T is the room temperature (commonly 298.15 K), R is the gas constant ($8.314\text{ J mol}^{-1}\text{ K}^{-1}$), $pH_{anode} - pH_{cathode}$ is the pH difference (ΔpH) of the two chambers, the theoretical applied voltage is only 0.404 V for electrochemical water electrolysis in a alkaline-acid electrolyzer with $\Delta pH = 14$, which greatly lowered the energy input for hydrogen production. Therefore, when the anode OER was replaced by urea oxidation reaction (UOR), the applied voltage can be further decreased, and the reactions and its corresponding Nernst equations can be expressed as following:

For water electrolysis in the base-acid electrolyzer with UOR replacing OER:

HER at the cathode:

The same as R1

UOR at the anode:



$$E_{UOR} = E_{UOR}^\theta - 2.303 \frac{RT}{6F} \log \left[\frac{(\alpha_{\text{CO(NH}_2)_2})(\alpha_{\text{OH}^-})^6}{(\alpha_{\text{N}_2})(\alpha_{\text{H}_2\text{O}})^5(\alpha_{\text{CO}_2})} \right] = 0.37\text{ V} - 0.059 * pH = -0.456 \quad ($$

$$E_{UOR}^\theta = 0.37\text{ V vs. RHE} \quad (\text{Eq.4})$$

The overall reaction:



$$V_{\text{Theory required or open circuit}} = E_{UOR}^\theta - E_{\frac{\text{H}^+}{\text{H}_2}}^\theta - 2.303 \frac{RT}{6F} \log \left[\frac{(\alpha_{\text{H}_2\text{O}})^5(\alpha_{\text{N}_2})(\alpha_{\text{H}_2})^3(\alpha_{\text{CO}_2})}{(\alpha_{\text{CO(NH}_2)_2})(\alpha_{\text{H}^+})^6(\alpha_{\text{OH}^-})^6} \right]$$

$$= 0.37 - 0.059 * (pH_{anode} - pH_{cathode}) = -0.456 \quad (\text{Eq.5})$$

According to the **Equation 5**, once the UOR replace the OER, the theoretical applied voltage is -0.456 V, suggesting that the as-proposed alkaline-acid electrolyzer can theoretically supply power with simultaneous hydrogen production. However, the electrolyzer still need applied voltage to drive the electrolysis H_2 production, owing to the overpotentials from the two half reactions, HER and UOR. Even so, coupling UOR with pH-gradient concentration cell, energy input for hydrogen production could largely be reduced compared with traditional water splitting.

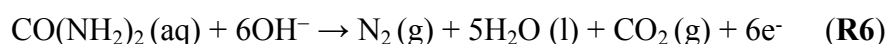
3. Theoretical Calculation Details

(1) DFT details

Spin-polarized DFT calculations were performed with periodic super-cells under the generalized gradient approximation (GGA) using the Perdew-Burke-Ernzerhof (PBE) functional for exchange-correlation and the ultrasoft pseudopotentials for nuclei and core electrons. The Kohn-Sham orbitals were expanded in a plane-wave basis set with a kinetic energy cutoff of 30 Ry and the charge-density cutoff of 300 Ry. The Fermi-surface effects have been treated by the smearing technique of Methfessel and Paxton, using a smearing parameter of 0.02 Ry. In modeling CuCl and CuO, 111 surfaces that are both considered to be the most closed pack surface are used. The periodically repeated three layer slab models with 2 x 2 supercell are introduced, while the topmost layer is allowed to relax during the structure optimization until the Cartesian force components acting on each atom were below 10^{-3} Ry/Bohr and the total energy converged to within 10^{-5} Ry. The Brillouin-zones were sampled with a $5 \times 5 \times 1$ k-point mesh. The PWSCF codes contained in the Quantum ESPRESSO distribution²⁰ were used to implement the calculations.

(2) Reaction model.

Basically, the reaction function of UOR is

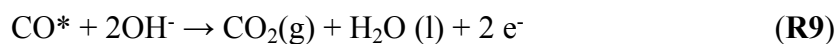
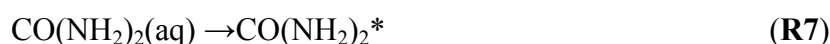


which contains a 6 electrons transfer. The equilibrium potential of **R6** is 0.37 V.

For the difficulty in directly modelling solvated urea, the Gibbs free energy of solvated urea is deduced by the DFT based free energy of $\text{N}_2(\text{g})$, $\text{H}_2\text{O}(\text{l})$, $\text{CO}_2(\text{g})$. The

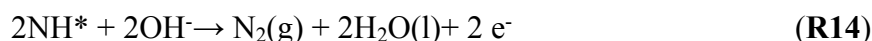
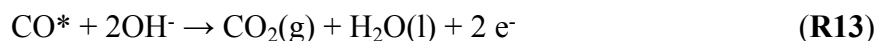
free energy of OH⁻ is calculated through the equilibrium of OH⁻+1/2H₂→H₂O(l)+e⁻ (basic hydrogen oxidation reaction) under $U_{\text{RHE}}=0$ V.

The associated key adsorbates during the reaction are urea molecule, NH₂ and CO. These key adsorbates are formed through the following reaction (asterisk denotes the adsorption species):



where the Gibbs free energy of adsorbates are calculated by the $G_{\text{A}^*} = G_{\text{A}^*+\text{slab}} - G_{\text{slab}} + \text{ZPE}_{\text{A}^*}$. ZPE_{A^*} stands for the zero point energy (ZPE) of adsorbate A*. The entropy terms are ignored for entropies are usually considered to be zero for the adsorbates. We have listed the corresponding entropies and ZPE on [Table S2](#).

As an alternative pathway to **R8**, the cracking of C-N is also possible to go through a proton couple electron transfer (PCET) process, which leads to the following pathway:



The reaction free energy diagram is shown on [Figure S23](#), which indicates a higher thermodynamic barrier than the direct cracking pathway (**R7-R10**), suggesting the

latter is more favorable practically. Besides, the side and top views of the optimized urea*, CO*, NH* and NH₂* on CuCl and CuO are shown on [Figure S24](#).

4. Faradic Efficiency for Hydrogen Production

The gas chromatograph equipped with a thermal conductivity detector (TCD) was used to analyze the production efficiency of H₂ in the UOR&HER electrolytic system and calculate the Faradaic efficiency. The calculation formula is expressed as below (**Eq.6**), α denotes the numbers of transferred electrons (*e.g.* $\alpha = 2$ for H₂), n denotes the number of moles of the obtained products, F is the faradaic constant, 96 485 C mol⁻¹, and Q denotes the whole passed charge. H₂ was collected by the chronopotentiometry experiment conducted at 10 mA cm⁻² in the homemade electrolyzer ([Figure S13b](#)) separated by a bipolar membrane with CuCl/rGO/CC as the anode in 1 M KOH and Pt/C/CC as the cathode in 0.5 M H₂SO₄. Before electrolyzing, Ar was introduced in the two chambers for 20 min and then the cell was sealed. The amounts of produced H₂ was analyzed every 10 min.

$$EF = \frac{\alpha n F}{Q} \quad (\text{Eq.6})$$

In these work, the whole passed charge Q could be obtained from the applied current and the maintained time, namely, $Q = I * t$, while n could be obtained by the the volum of obtained H₂ (V), *i.e.*, $n = V/24.5$, (24.5 L mol⁻¹ is the gas constant at 25 °C), and the V can be quantitatively determined by the GC analysis. The actual equation can be expressed as following:

$$EF = \frac{V \alpha F}{24.5 * I t} \quad (\text{Eq. 7})$$

5. Figures

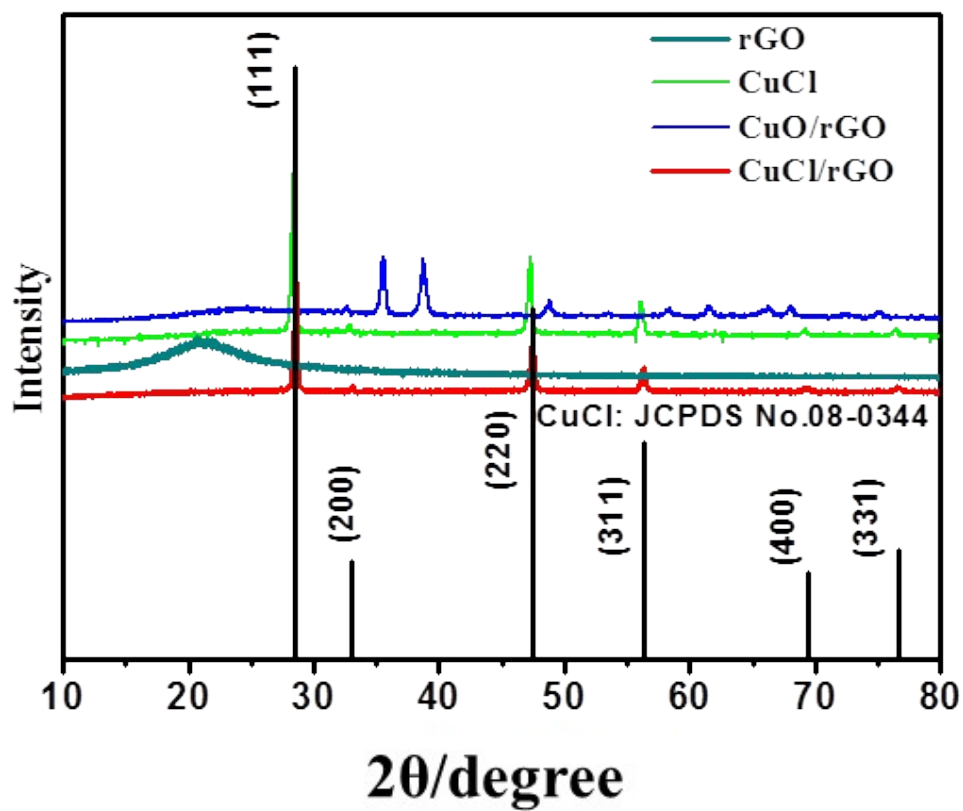
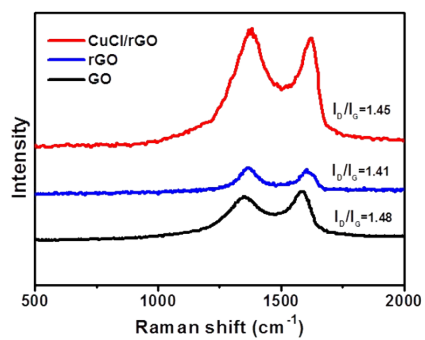


Figure S1. XRD patterns for rGO, CuCl, CuCl/rGO, and CuO/rGO.



Compounds	I_D (integral area)	I_G (integral area)	I_D/I_G
CuCl/rGO	23454.32	16112.35	1.45
rGO	8947.96	6347.04	1.41
GO	9121.49	6156.40	1.48

Figure S2. Raman spectra for CuCl/rGO, rGO, and GO

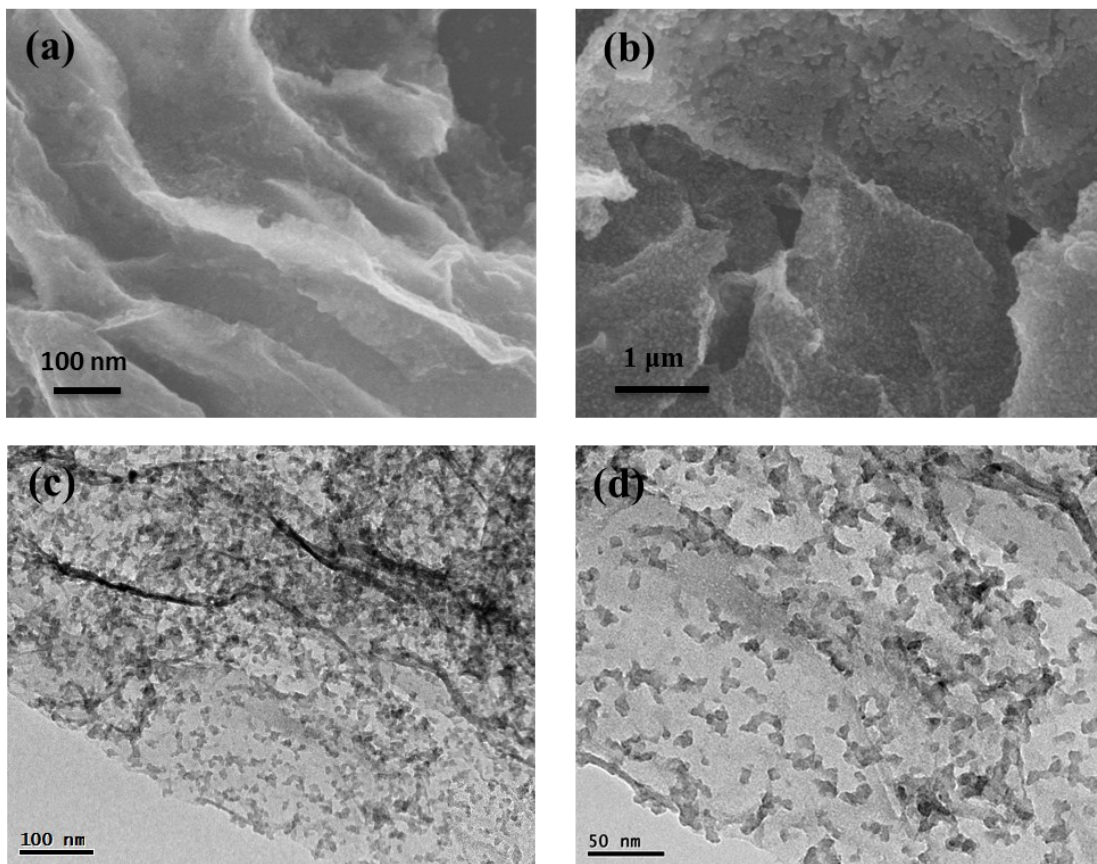


Figure S3. SEM (a) and (b), and TEM images(c) and (d) for CuCl/rGO

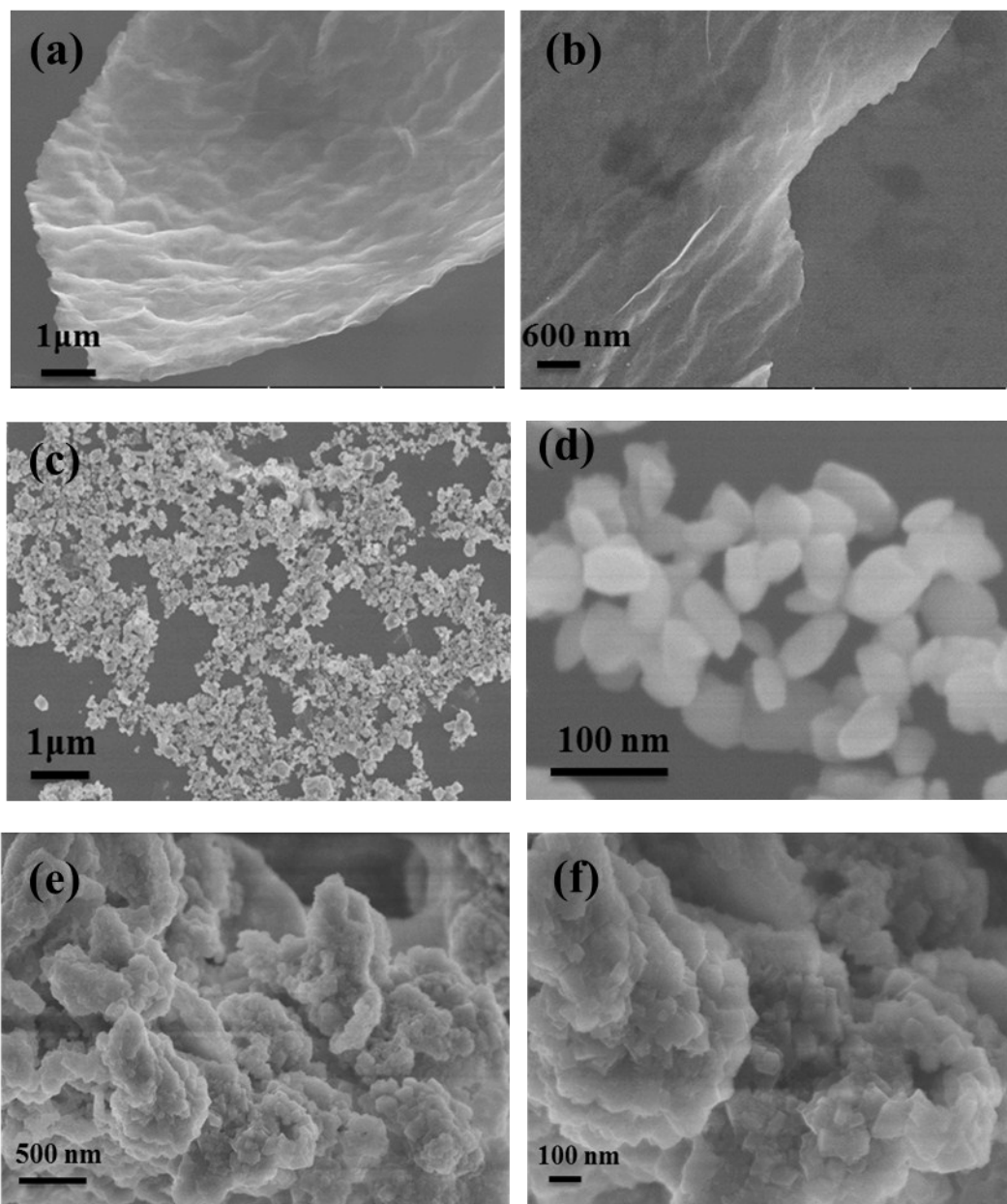


Figure S4. SEM images for rGO (a) and (b), CuCl c) and (d), and reagent CuCl (e) and (f)

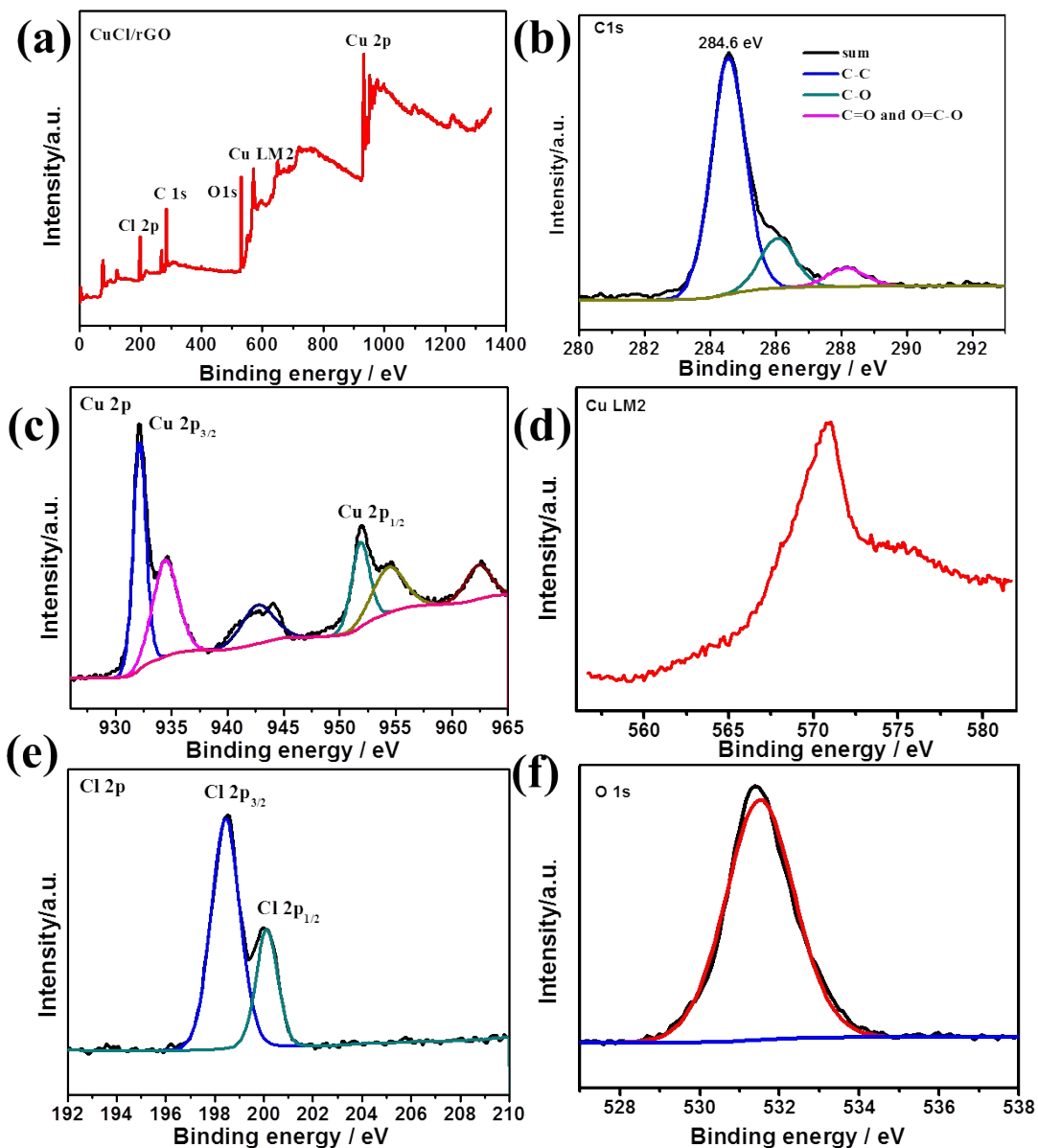


Figure S5. XPS spectra of CuCl/rGO

Note: Combined with the Auger Cu LMM (binding energy of 570.9 eV) and Cu 2p spectra, the peaks at around 932.2 eV and 951.9 eV can be assigned to the binding energies of Cu(I).⁴ While the peaks at 934.5 eV and 954.4 eV suggest the presence of Cu(II) which may derive from the exposure to air.

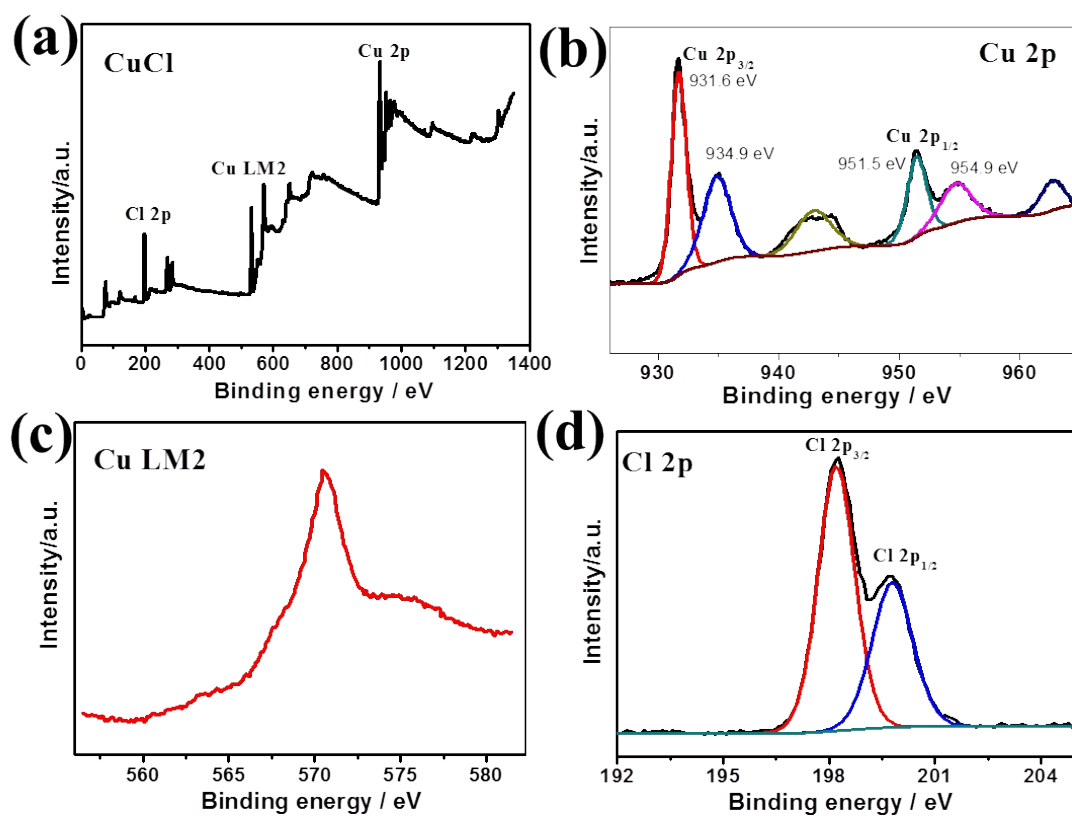


Figure S6. XPS spectra of CuCl

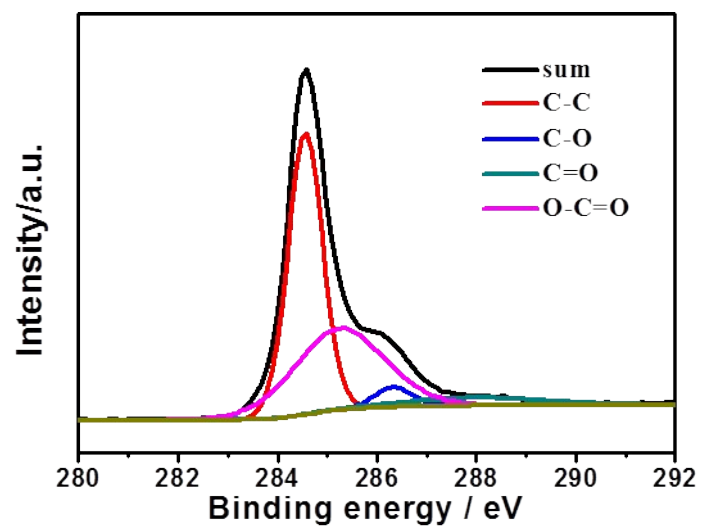


Figure S7. XPS spectra of rGO

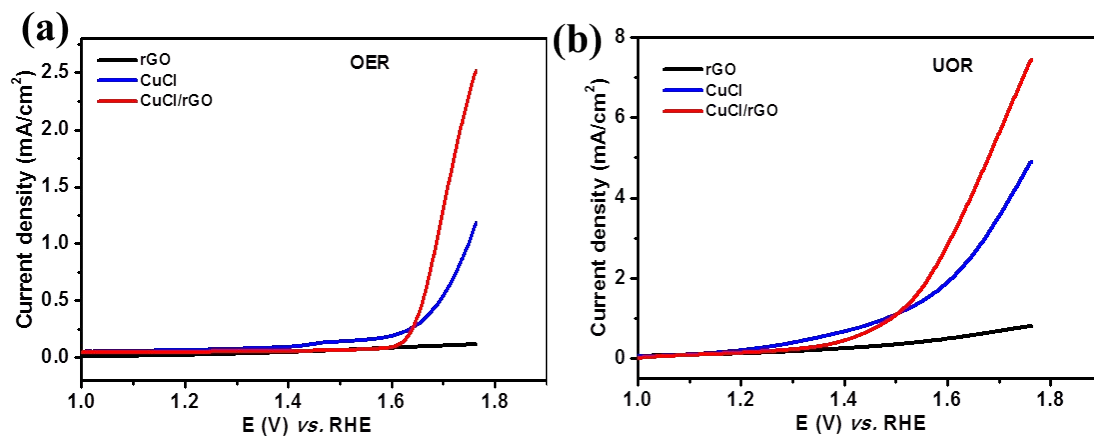


Figure S8. LSV curves of CuCl/rGO, CuCl and rGO in 1.0 M KOH electrolyte in the absence (a) and presence (b) of 0.5 M urea at 10 mV s^{-1}

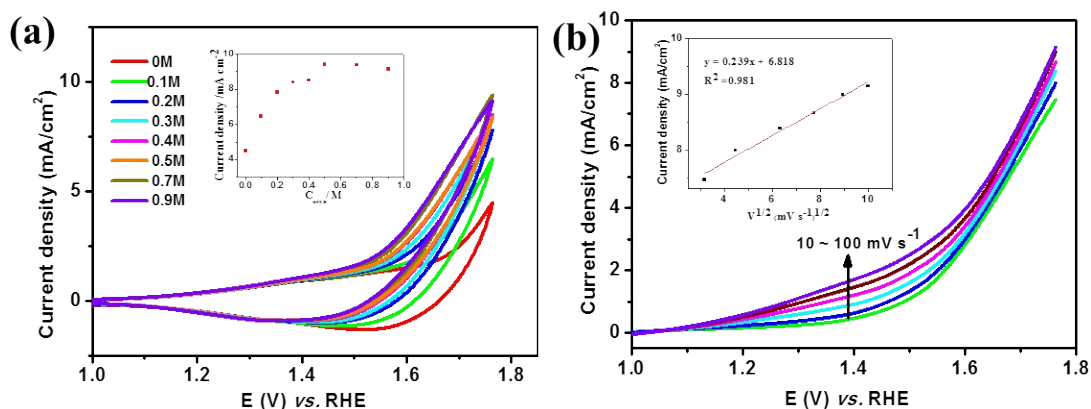


Figure S9. (a) Cyclic voltammogram of the CuCl/rGO electrode in 1 M KOH with different urea concentration at 50 mV s^{-1} ; (b) LSV of the CuCl/rGO electrode in 1 M KOH with 0.5 M urea at different scan rates.

Note: Cyclic voltammogram was performed to investigate the electrochemical response to varied urea concentration at the CuCl/rGO electrode (Figure S9a), That the anodic current is independent of urea concentration at higher concentration ($> 0.5 \text{ M}$, inset in Figure S9a) may be attributed to the kinetics limitation control process, which could be interpreted as that the catalyst surface was covered by urea molecules in a high urea concentration resulting in no change of oxidation rate owing to lack of local OH^- for spare urea molecules.⁵ Figure S9b displays the LSV curves for CuCl/rGO electrode at different scan rates, in which the peak current density followed a linear relation with the square root of the scan rates ($R^2 = 0.981$), further confirming that UOR on the CuCl/rGO electrode is a diffusion-controlled process.⁶

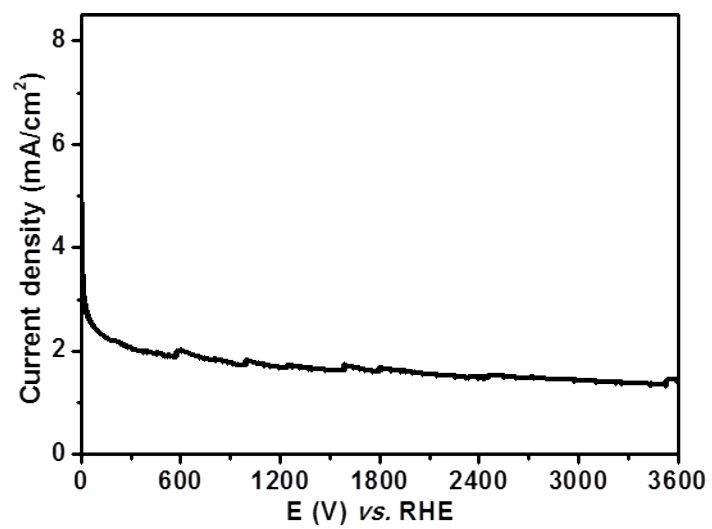


Figure S10. CA curve of the CuCl/rGO electrode in 1 M KOH with 0.5 M urea at 1.56 V vs. RHE

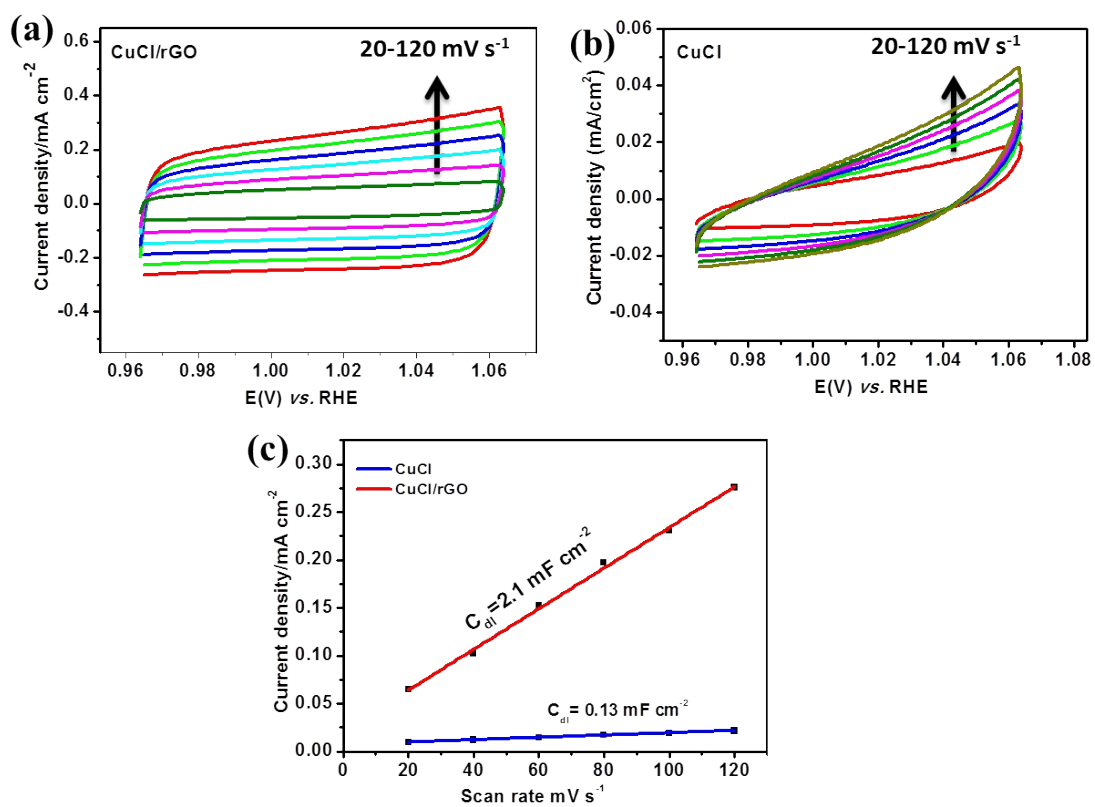


Figure S11. Electrochemical capacitance measurements for the estimation of the electrochemical active surface area of catalysts; Cyclic voltammograms of the CuCl/rGO (a) and CuCl (b); the extraction of the double-layer capacitances of CuCl/rGO and CuCl (c)

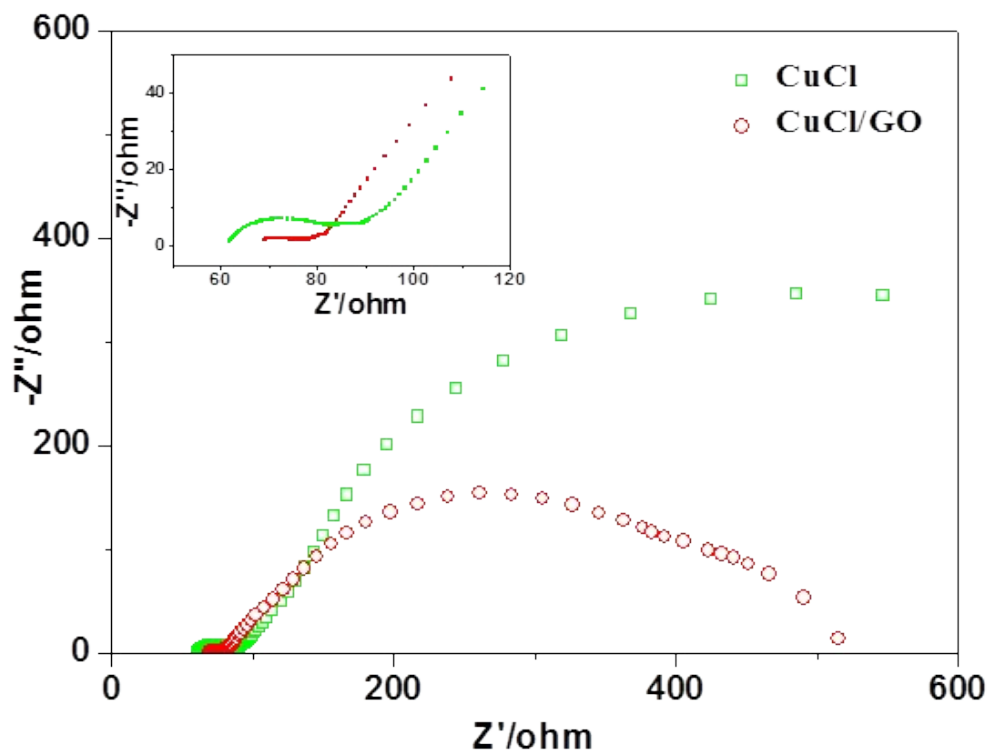


Figure S12. Nyquist plots of CuCl/rGO and CuCl in 1 M KOH with 0.5 M urea

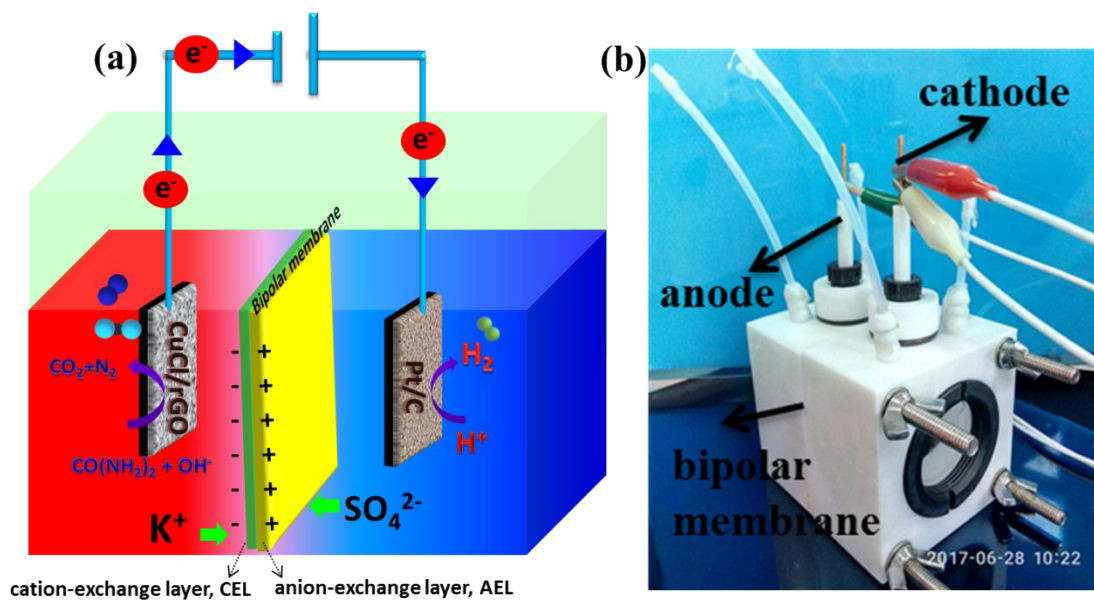


Figure S13. The operating principle and schematic map of the bipolar membrane as the separator based on the UOR&HER (a) and the digital photo for the homemade asymmetric-electrolyte electrolyzer (b).

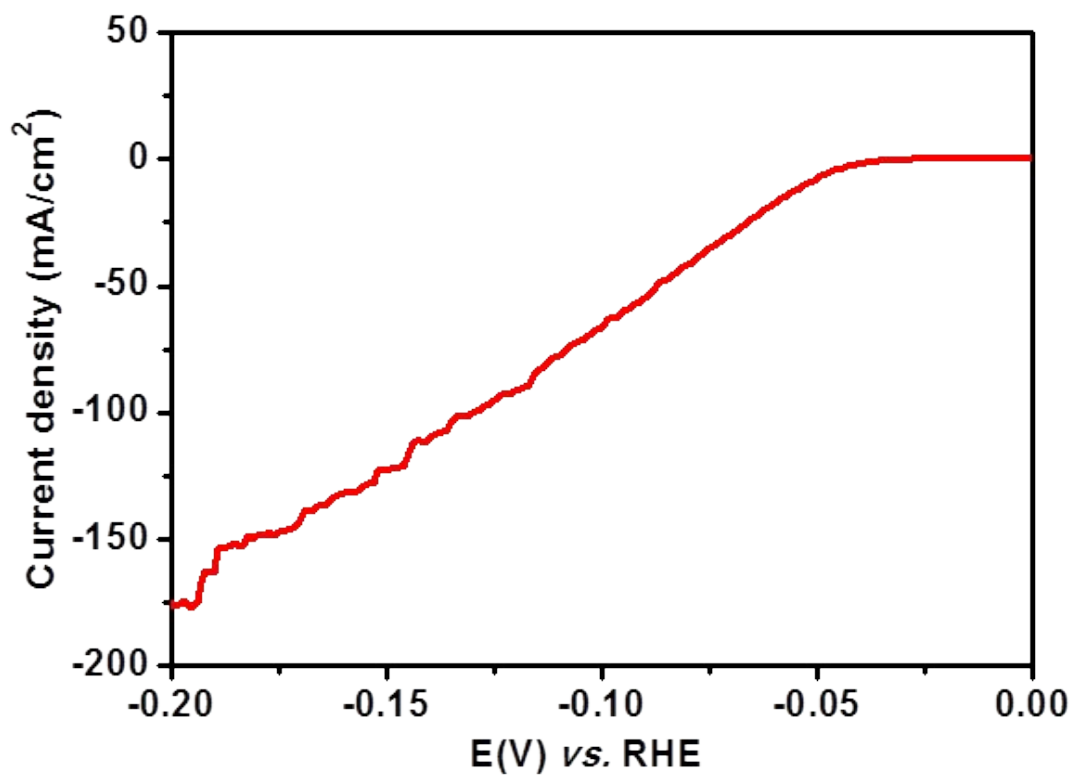


Figure S14. LSV curves for Pt/C in 0.5 M H₂SO₄ at 5 mV s⁻¹

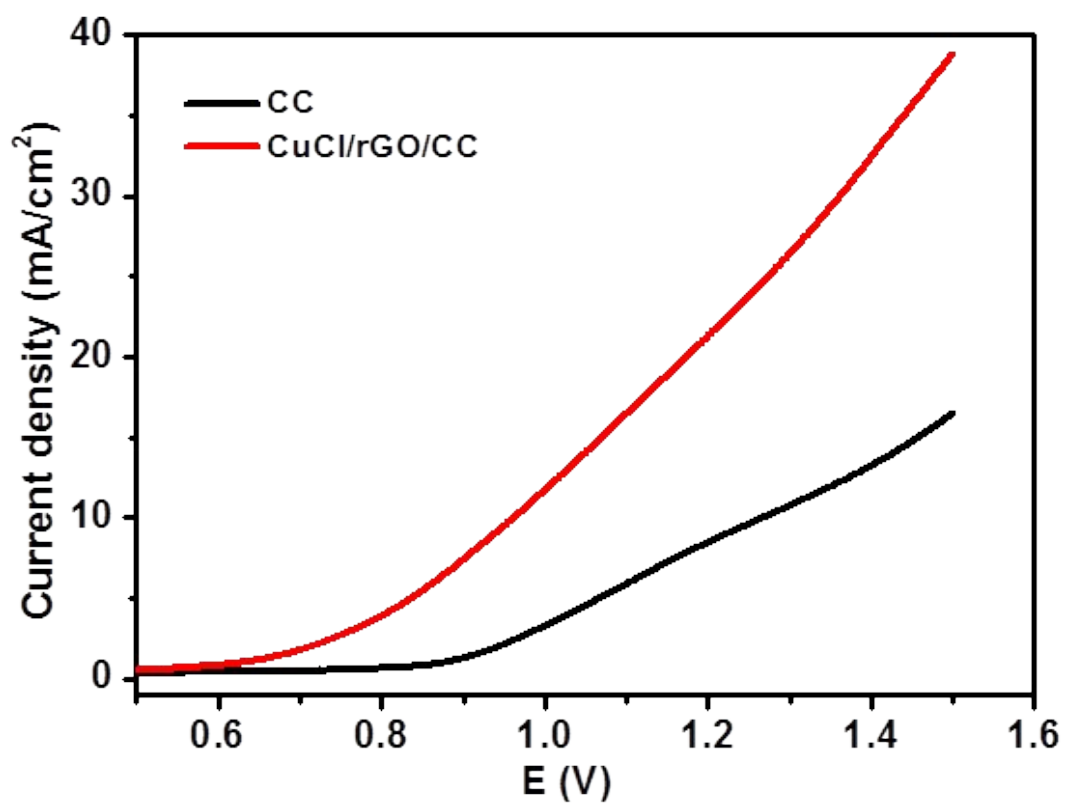


Figure S15. LSV curves for the HER&UOR electrolyzer with CuCl/rGO/CC or CC as the anode electrodes in 1.0 M KOH and Pt/C as the cathode electrode in 0.5 M H₂SO₄ with 0.5 M urea at 5 mV s⁻¹

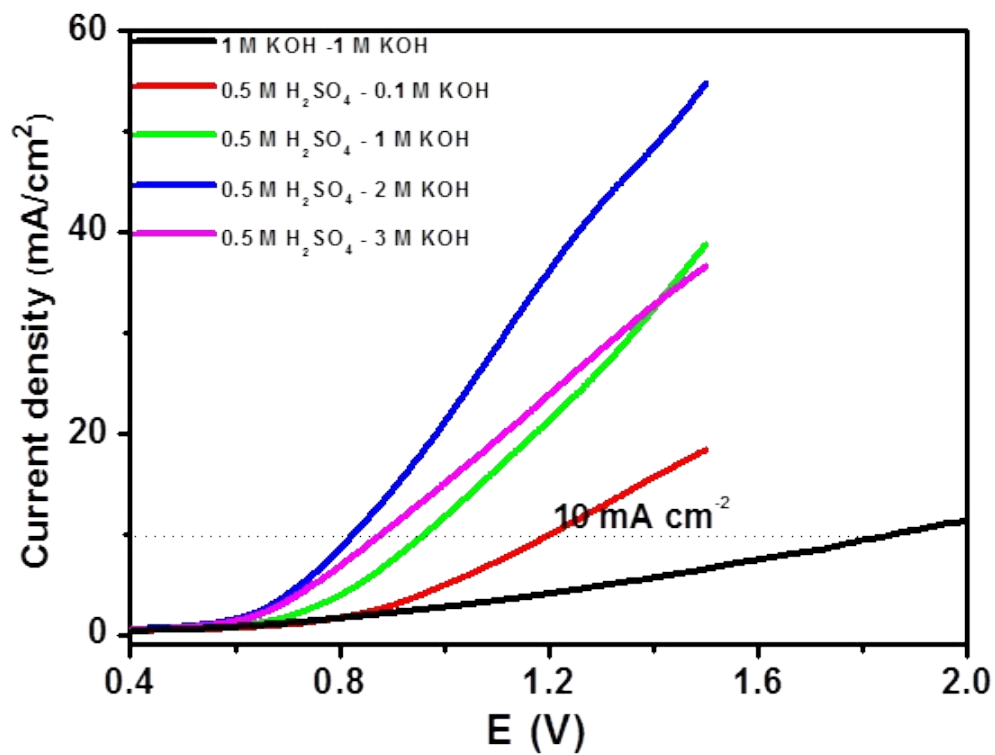


Figure S16. LSV curves for the HER&UOR electrolyzer with CuCl/rGO/CC and Pt/C/CC as the electrodes under different pH differences in the presence of 0.5 M urea at 5 mV s⁻¹

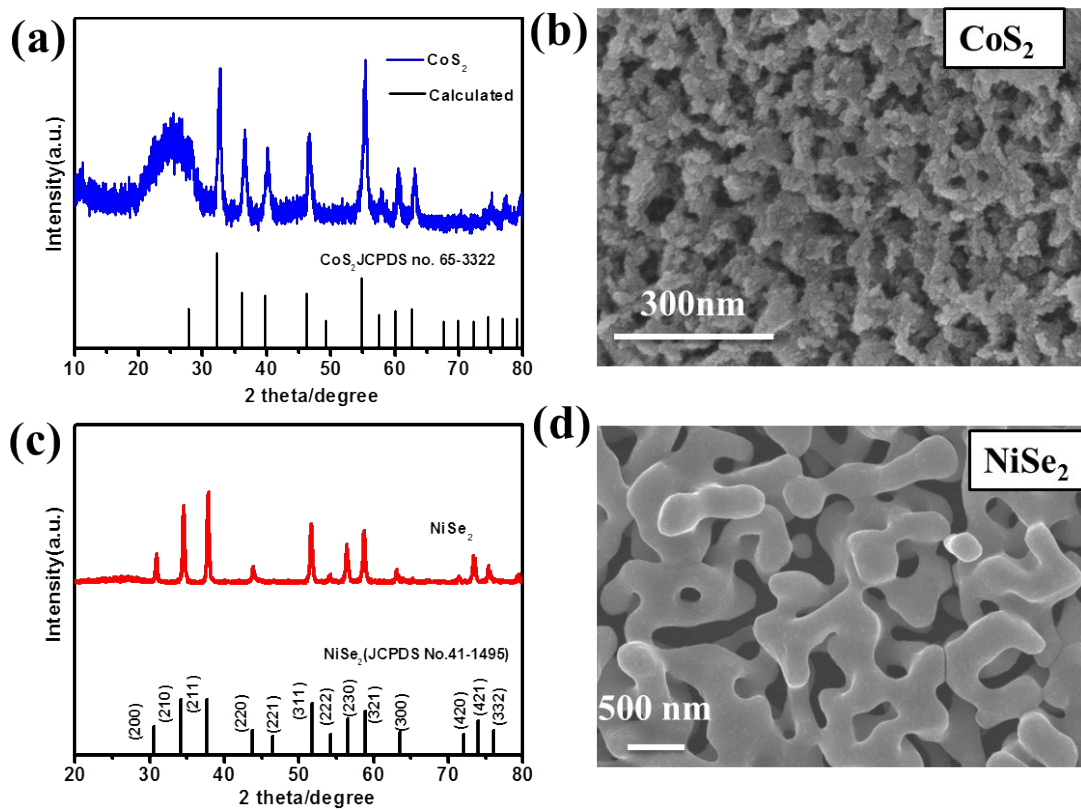


Figure S17. XRD patterns and SEM images for CoS_2 and NiSe_2

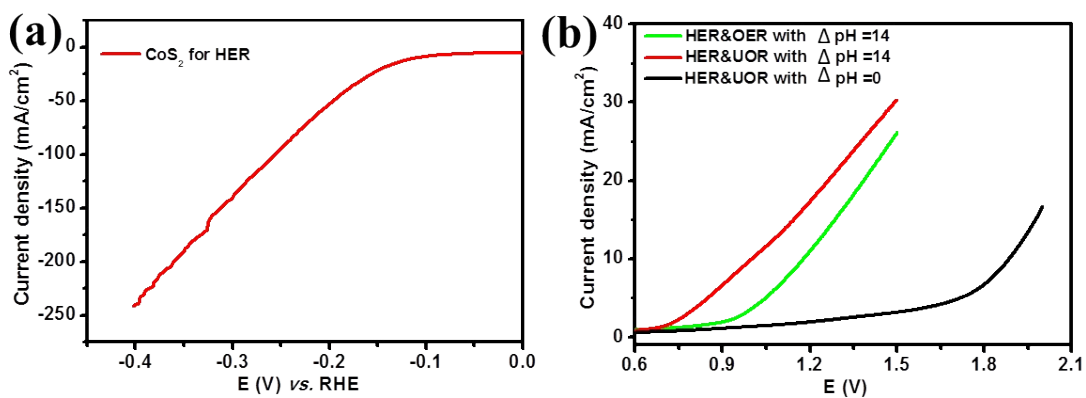


Figure S18. (a) LSV of CoS₂ for HER at 5 mV s⁻¹; (b) LSV curves of the electrolyzer with CuCl/rGO as the anode for UOR or OER, and CoS₂ as the cathode for HER at 5 mV s⁻¹;

Note: Figure S18a shows CoS₂ could drive 10 mA cm⁻² at overpotential of 110 mV in 0.5 M H₂SO₄ for HER. The asymmetric-electrolyte electrolyzer (ΔpH = 14) assembled with CoS₂ as the cathode for HER and CuCl/rGO/CC as the anode for UOR also achieved energy-saving hydrogen production assisted by UOR and pH difference, delivering 10 mA cm⁻² at 1.0 V (Figure S18b).

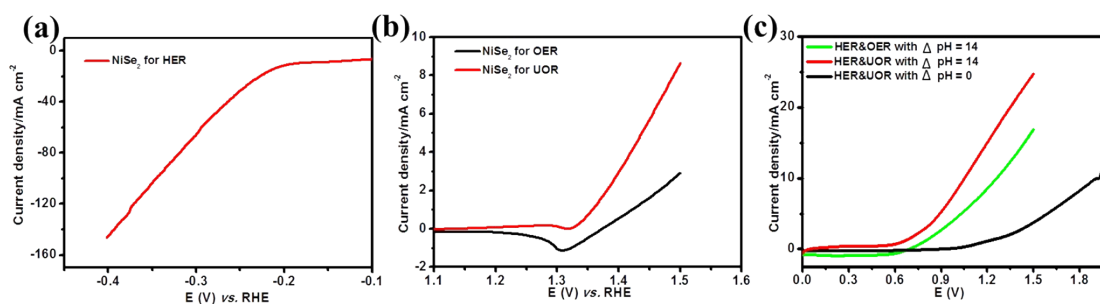


Figure S19. (a) LSV curves of NiSe₂ for HER in 0.5 M H₂SO₄ at 5 mV s⁻¹; (b) LSV curves of NiSe₂ for UOR and OER in 1.0 M KOH with or without 0.5 M urea at 5 mV s⁻¹ (c) LSV curves for the asymmetric-electrolyte or single electrolyte electrolyzer at 5 mV s⁻¹ with NiSe₂ as the bifunctional catalysts.

Note: As shown in [Figure S19](#), the NiSe₂ nanocoral ([Figure S17c-d](#)) acts as the bifunctional catalyst for HER and UOR, showing a potential of 186 mV to drive 10 mA cm⁻² for HER in 0.5 M H₂SO₄ ([Figure S19a](#)), and launch UOR at about 1.30 V in 1.0 M KOH with 0.5 M urea ([Figure S19b](#)). The NiSe₂/CC electrodes were applied in the asymmetric-electrolyte electrolyzer, the required voltage for water electrolysis is greatly reduced with assistance of UOR and pH difference, only requiring 1.05 V to drive 10 mA cm⁻² ([Figure S19c](#)). Confirmed by the experiments presented in [Figure S18 and S19](#), the catalysts for UOR and HER could be replaced by other catalysts except the CuCl/rGO and Pt/C, therefore, the designed asymmetric-electrolyzer can work generally.

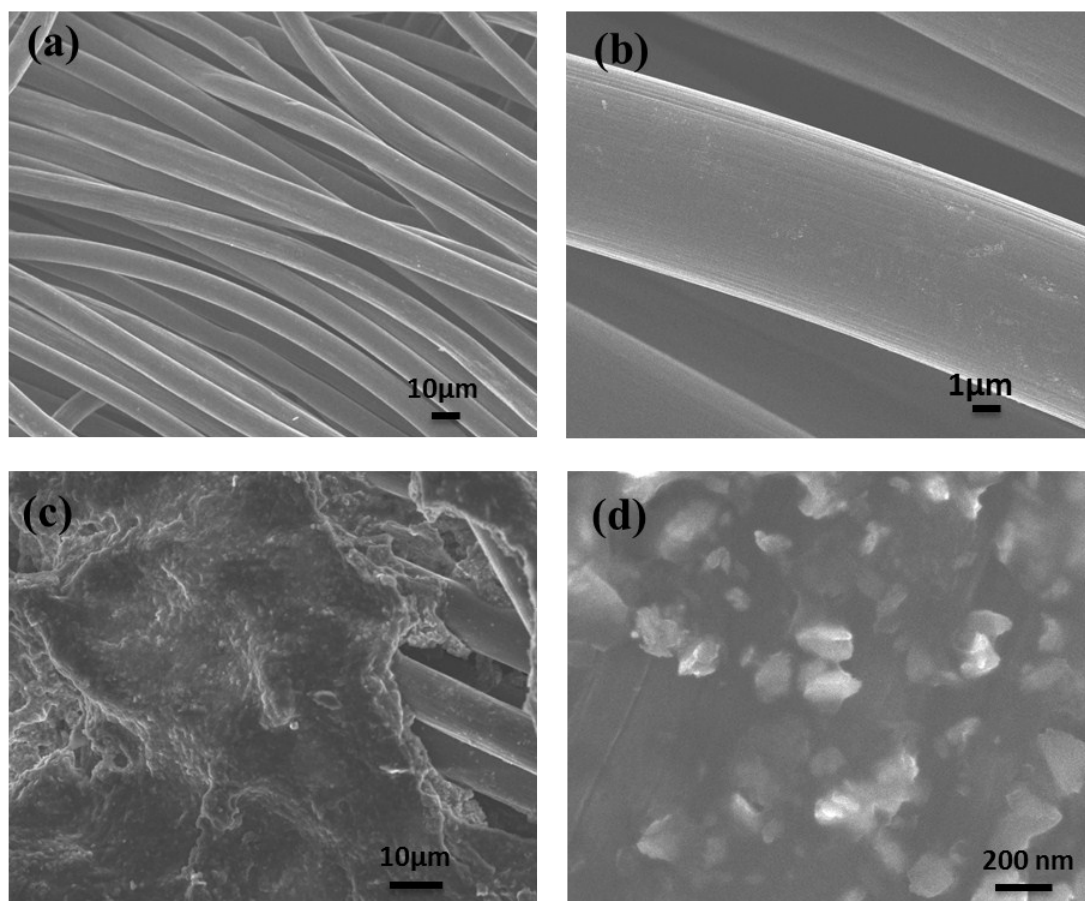


Figure S20. SEM images of carbon cloth (a) and (b), and CuCl/rGO post-urea oxidation on carbon cloth (c) and (d) at different magnifications

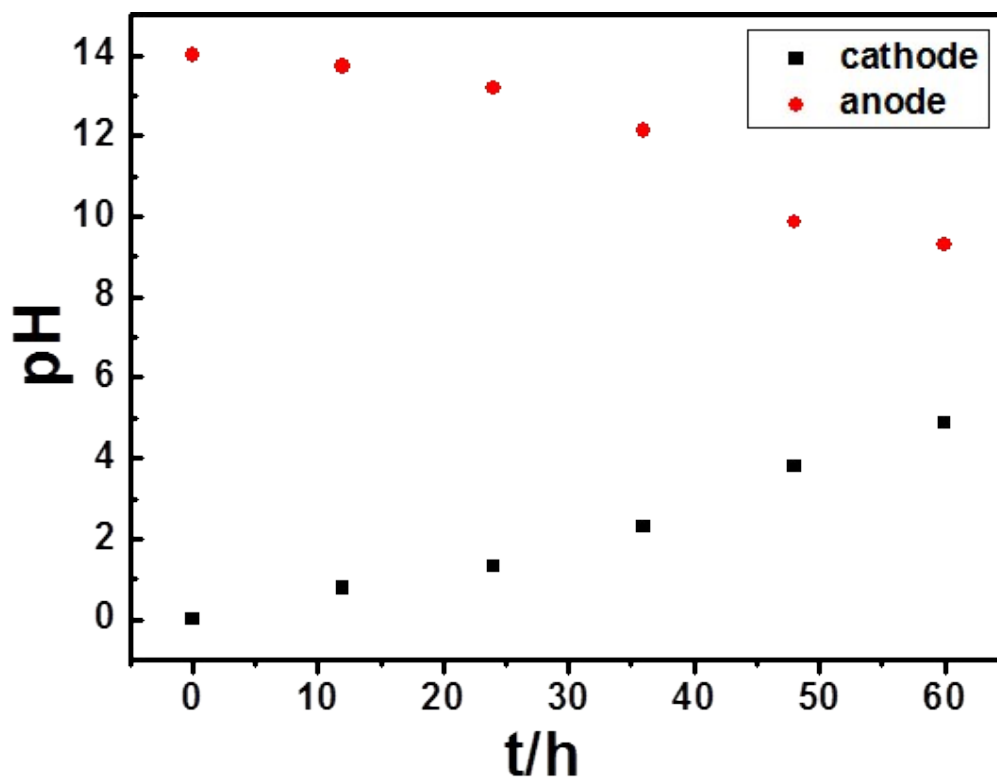


Figure S21. Monitoring the changes of the pH values in the cathode and anode at a discharge current density of 10 mA cm^{-2} .

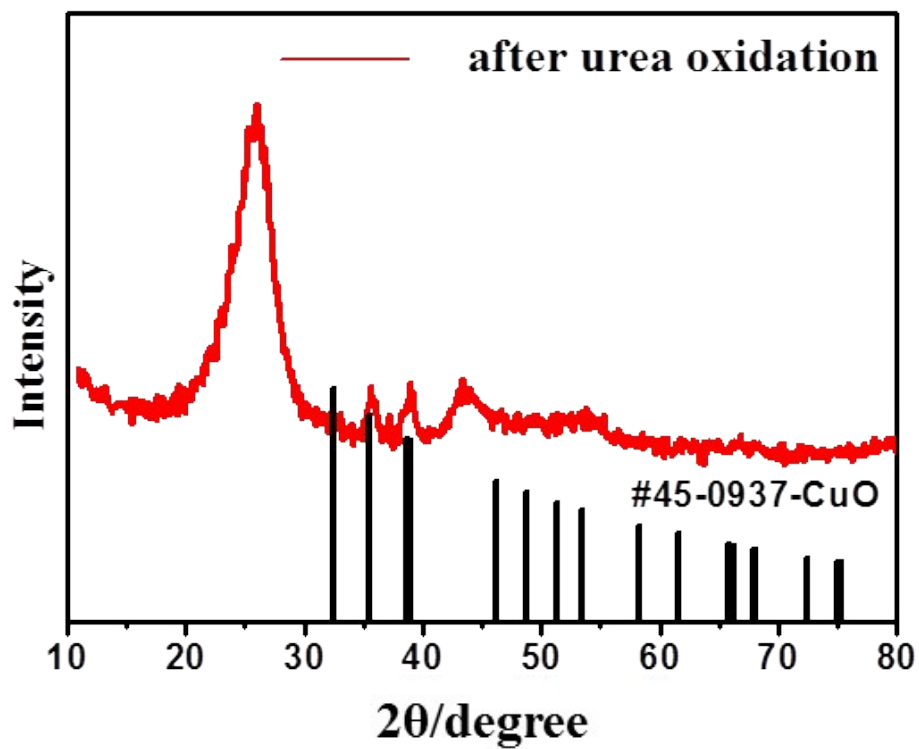


Figure S22. XRD patterns of CuCl/rGO post-urea oxidation on carbon cloth

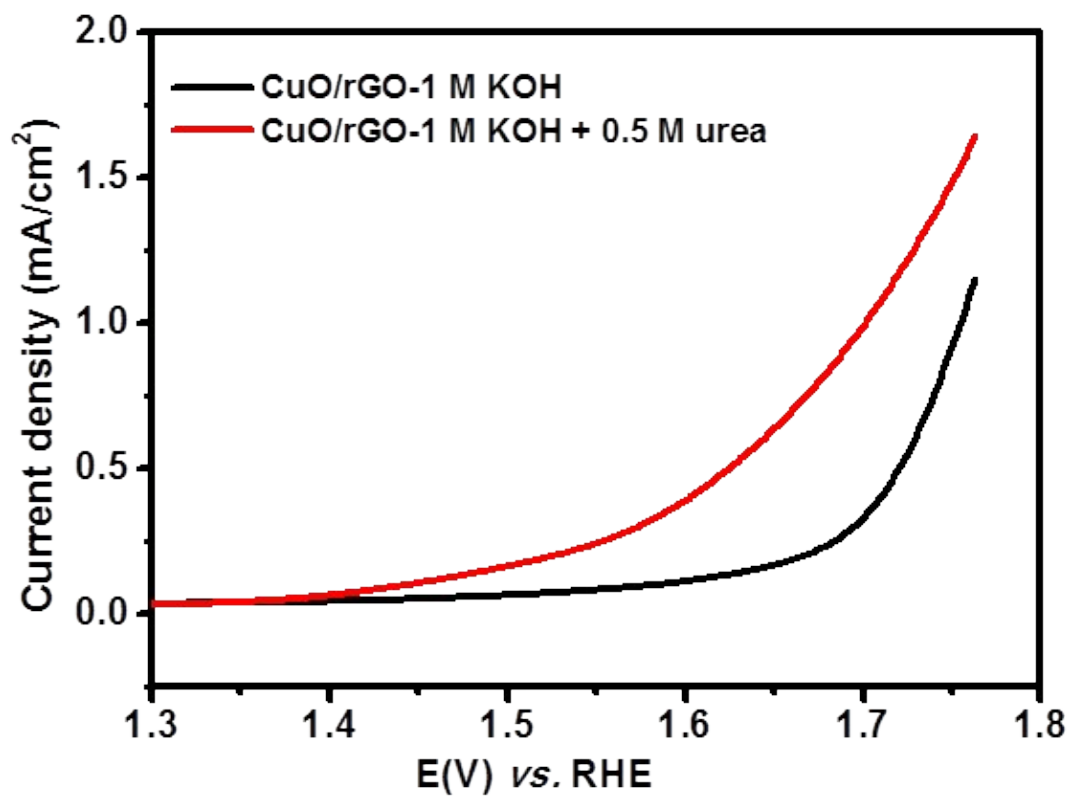


Figure S23. LSV of the CuO/rGO electrode in 1 M KOH with or without 0.5 M urea at a scan rate of 10 mV s⁻¹

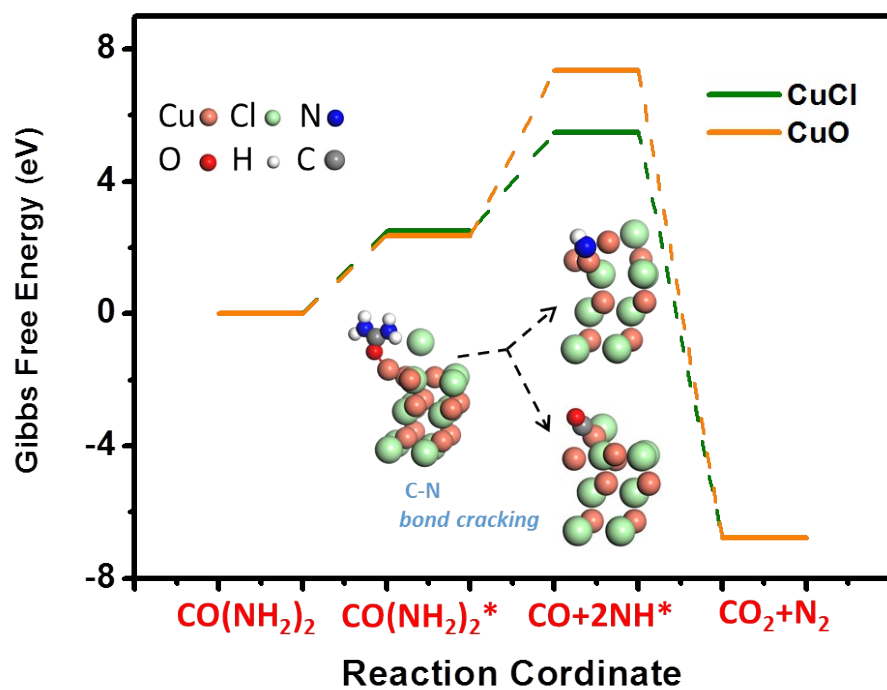


Figure S24. The reaction free energy diagram of C-N PCET cracking, with the formation of NH^*

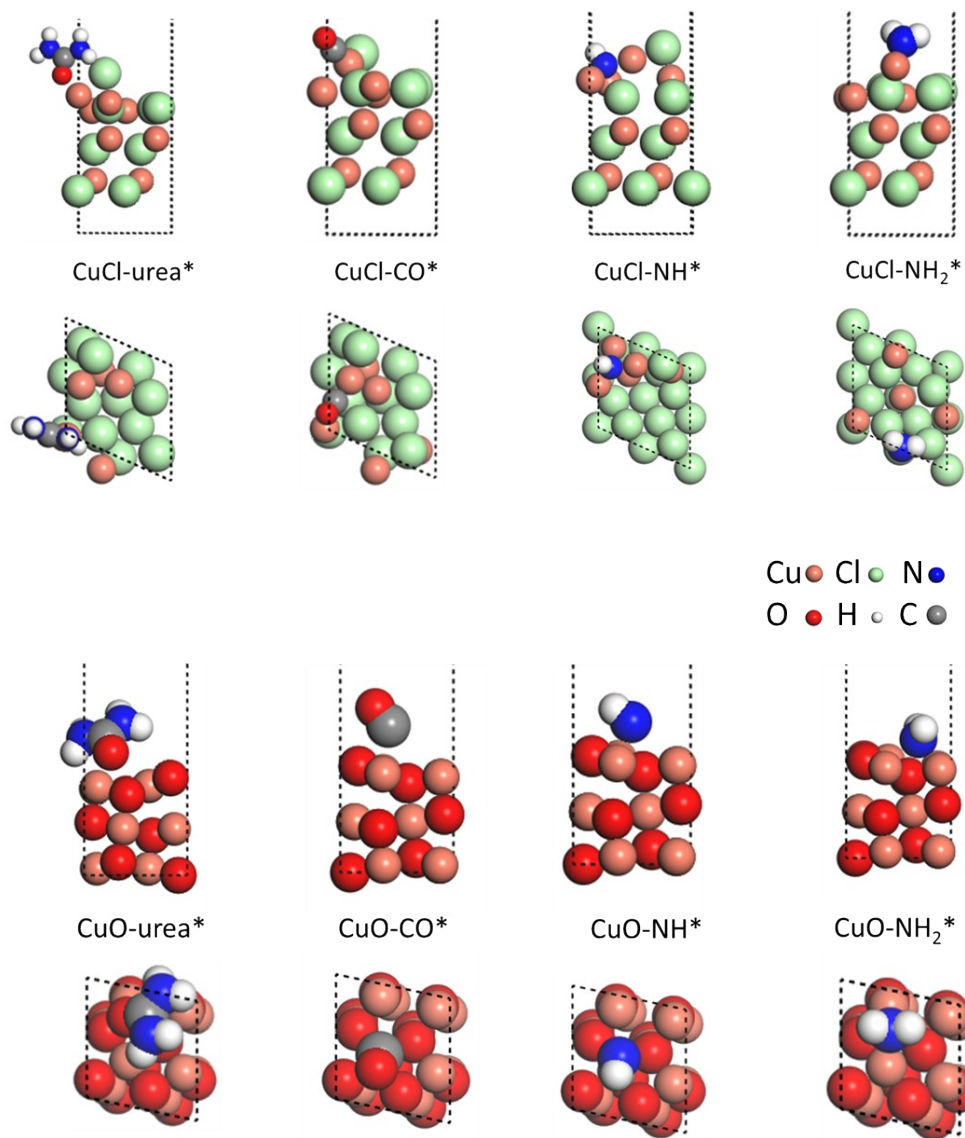


Figure S25. The side and top views of the optimized structures of the possible reaction intermediates

6. Tables

Table S1. Comparison of the reported double-cell with biomass oxidation and single-cell with urea oxidation in recent two years

Catalysts	Anodic oxidation	Electrolytes	Applied voltage at 10 mA cm ⁻² /(V)	Refs
Ni ₃ S ₂ /NF ^d	10 mM HMF	1.0 M KOH	1.46	7
Ni ₂ P NPA/NF ^d	10 mM HMF	1.0 M KOH	1.44	8
Co-P/CF ^d	10 mM HMF	1.0 M KOH	1.39 ^m	9
hp-Ni ^d	Benzyl alcohol	1.0 M KOH	1.50	10
Ni ₂ P/Ni/NF ^d	30 mM furfural	1.0 M KOH	1.48	11
3D PdCu alloy NSs ^d	1.0 M Ethanol	1.0 M KOH	NG	12
Ultrathin Co ₃ O ₄ NSs ^d	1.0 M Ethanol	1.0 M KOH	NG	13
Zn _{0.08} Co _{0.92} P ^s	0.5 M urea	1.0 M KOH	1.38	14
Ni ₂ P NF/CC ^s	0.5 M urea	1.0 M KOH	1.15 ^m	15
MnO ₂ /MnCo ₂ O ₄ /Ni ^s	0.5 M urea	1.0 M KOH	1.58	16
Small-sized MnO ₂ ^s	0.5 M urea	1.0 M KOH	1.41	17
CoS ₂ NA/Ti ^s	0.3 M urea	1.0 M KOH	1.59	18
Ni ₃ N nanosheet/CC	0.33 M urea	1.0 M KOH	1.44	19
CuCl/rGO ^d	0.5 M urea	1.0 M KOH and 0.5 M H ₂ SO ₄	0.96	this work
	0.5 M urea	2.0 M KOH and 0.5 M H ₂ SO ₄	0.83	this work

HMF: 5-hydroxymethylfurfural,

CC: Carbon cloth

d: double-cell

s: single-cell

m: evaluated in its figures

NG: not given

Table S2. The zero-point energy (ZPE) values are calculated with the Phonon-5.0.2 module in espresso-5.0,²¹ and the molecular entropy values are from Ref. 21. A pressure of 0.035 Bar is included in the entropy of gas-phased H₂O, for at 300 K, gas-phased H₂O and the liquid water reach equilibrium under this pressure.

Species	TS (eV)	ZPE (eV)
H ₂ (g)	0.41	0.27
H ₂ O(g)	0.67	0.59
N ₂ (g)	0.61	0.17
CO ₂ (g)	0	0.75
CO(NH ₂) ₂ *	0	1.99
NH*	0	0.32
CO*	0	0.13

7. References

References:

1. Hummers Jr, W. S.; Offeman, R. E. *J. Am. Chem. Soc.* 1958, **80**, 1339-1339.
2. McDonald, M. B.; Ardo, S.; Lewis, N. S.; Freund, M. S.; *Chemsuschem* 2014, **7**, 3021-3027.
3. Schreier, M.; Héroguel, F.; Steier, L.; Ahmad, S.; Luterbacher, J. S.; Mayer, M. T.; Luo, J.; Grätzel, M.; *Nat. Energy* 2017, **2**, 17087.
4. Huan, T. N., Simon, P.; Benayad, A.; Guetaz, L.; Artero, V.; Fontecave, M. *Chem. – Eur. J.* 2016, **22**, 14029-14035.
5. Barakat, N. A. M., El-Newehy, M. H.; Yasin, A. S.; Ghouri, Z. K.; Al-Deyab, S. S. *Appl. Catal. A-Gen.* 2016, **510**, 180-188.
6. Boggs, B. K.; King, R. L.; Botte, G. G. *Chem. Commun.* 2009, **32**, 4859-4861.
7. You, B.; Liu, X.; Jiang, N.; Sun, Y. *J. Am. Chem. Soc.* 2016, **138**, 13639-13646.
8. You, B.; Jiang, N.; Liu, X.; Sun, Y. *Angew. Chem. Int. Ed.* 2016, **128**, 10067-10071.
9. Jiang, N.; You, B.; Boonstra, R.; Terrero Rodriguez, I. M.; Sun, Y. *ACS Energy Lett.* 2016, **1**, 386-390.
10. You, B.; Liu, X.; Liu, X.; Sun, Y. *ACS Catal.* 2017, **7**, 4564-4570.
11. Jiang, N.; Liu, X.; Dong, J.; You, B.; Liu, X.; Sun, Y. *ChemNanoMat* 2017, **3**, 491-495.
12. Zhao, X.; Dai, L.; Qin, Q.; Pei, F.; Hu, C.; Zheng, N. *Small* 2017, **13**, 1602970.
13. Dai, L.; Qin, Q.; Zhao, X.; Xu, C.; Hu, C.; Mo, S.; Wang, Y. O.; Lin, S.; Tang, Z.; Zheng, N. *ACS Cent. Sci.* 2016, **2**, 538-544.
14. Liu, T.; Liu, D.; Qu, F.; Wang, D.; Zhang, L.; Ge, R.; Hao, S.; Ma, Y.; Du, G.; Asiri, A. M.;

- Chen, L.; Sun, X. *Adv. Energy Mater.* 2017, **1700020**.
15. Liu, D.; Liu, T.; Zhang, L.; Qu, F.; Du, G.; Asiri, A. M.; Sun, X. *J. Mater. Chem. A* 2017, **5**, 3208-3213.
16. Xiao, C.; Li, S.; Zhang, X.; MacFarlane, D. R. *J. Mater. Chem. A*, 2017, **5**, 7825-7832.
17. Chen, S.; Duan, J.; Vasileff, A.; Qiao, S. Z. *Angew. Chem. Int. Ed.* 2016, *128*, 3868-3872.
18. Wei, S.; Wang, X.; Wang, J.; Sun, X.; Cui, L.; Yang, W.; Zheng, Y.; Liu, J.; *Electrochim. Acta* 2017, **246**, 776-782.
19. Liu, Q.; Xie, L.; Qu, F.; Liu, Z.; Du, G.; Asiri, A. M.; Sun, X. *Inorg. Chem. Front.* 2017, **4**, 1120-1124.
20. Giannozzi, P.; Bonini, S. B. N.; Calandra, M.; Car, R.; Cavazzoni, C.; Ceresoli, D.; Chiarotti, G. L.; Cococcioni, M.; Dabo, I.; Dal Corso, A.; Fabris, S.; Fratesi, G.; de Gironcoli, S.; Gebauer, R.; Gerstmann, U.; Gougoussis, C.; Kokalj, A.; Lazzeri, M.; MartinSamos, L.; Marzari, N.; Mauri, F.; Mazzarello, R.; Paolini, S.; Pasquarello, A.; Paulatto, L.; Sbraccia, C.; Scandolo, S.; Sclauzero, G.; Seitsonen, A. P.; Smogunov, A.; Umari, P.; Wentzcovitch, R. M. QUANTUM ESPRESSO: a modular and open-source software project for quantum simulations of materials. *J. Phys.: Condens. Matter* 2009, **21**, 395502.
21. Weast, R. C., Ed. CRC Handbook of Chemistry and Physics, 49th ed.; The Chemical Rubber Company: Cleveland, OH, 1968-1969; **p D109**.